Potential of N2 /O2 Atmospheric Pressure Needle-Water DC Microplasmas for nitrogen fixation: nitrite-free synthesis of nitrates

Cédric Pattyn, Nicolas Maira, Antoine Remy, Nepal Chandra Roy, Sylvain Iséni, David Petitjean, François Reniers

*C. Pattyn et. al., RSC PCCP, 2020, **22**, 24801-24812.*
The Version of Record is available online at doi:10.1039/D0CP03858J.

Potential of N_2/O_2 Atmospheric Pressure Needle-Water DC Microplasmas for nitrogen fixation: nitrite-free synthesis of nitrates

C. Pattyn[a*], N. Maira[a], A. Remy[a], N. C. Roy[a], S. Iseni[b], D. Petitjean[a] and F. Reniers[a]

[a]*Université Libre de Bruxelles, Faculty of Sciences, Chemistry of Surfaces Interfaces and Nanomaterials (ChemSIN), Avenue F. D. Roosevelt 50, B-1050 Brussels, Belgium.*
[b]*GREMI – Groupe de Recherches sur l'Energétique des Milieux Ionisés, UMR 7344 CNRS/Université d'Orléans, 14 rue d Issoudun, BP6744, 45067 Orléans Cedex 2, France.*

[*]*Corresponding author: cedric.pattyn.pro@protonmail.com*

Received 20th July 2020, Accepted 14th October 2020, published 17th November 2020.
Volume 22, Issue 42, p. 24801-24812

Abstract

A needle-water DC microplasma system working at atmospheric pressure in N_2/O_2 gas mixtures is used to study the fundamental mechanisms of nitrates/nitrites synthesis in highly complex and yet little-known plasma-water systems. Plasma properties are investigated by means of optical emission spectroscopy while the activated water is analyzed following the treatment using ionic chromatography and UV-Vis absorbance spectroscopy. Experiments highlight that the energy efficiency and selectivity of the process are influenced by the oxygen content and the plasma-induced water heating, with strong differences when the water surface is the anode or the cathode electrode. Nitrates are successfully synthesized without residual nitrites in the solution with a comparatively higher energy efficiency when the water is the cathode. The possible reactions involved in the gas phase and aqueous phase chemistry are presented and future scopes for the optimization of the system are discussed.

Introduction

Nitrogen is an essential element for all forms of life on earth. In agriculture, the three main macronutrients used in fertilizers are based on nitrogen (N), phosphorus (P) and potassium (K). While nitrogen is the most abundant element in our environment (78% of earth atmosphere), it is the least available to living organisms due to its natural form of N_2 molecules. Breaking the triple bond between two nitrogen atoms requires a significant amount of energy (9.79eV)[1]. Therefore, before being involved in biological reactions (as e.g. for proteins or DNA building) or used in industrial processes, nitrogen atoms must be bonded to other elements in order to provide accessible compounds such as nitrates (NO_3^-) or ammonia (NH_3). The nitrogen fixation (NF) is naturally carried out via lightning (converting N_2 and O_2 into NO_x which can later react with water to form nitric acid or nitrates) and by micro organisms. It is also artificially implemented using the Haber-Bosch/Ostwald processes though ammonia synthesis and conversion to nitric acid.

The development of the Haber-Bosch process has been an enormous technological breakthrough, allowing fixing nitrogen industrially on a large scale and impacting deeply the global nitrogen cycle in the last century[2–5]. However, although it has been extensively optimized, the energy efficiency has almost reached the theoretical limit and its global environmental impact remains significant. The Haber-Bosch process alone spends 1-2% of the global energy consumption and releases 300 million tons of fossil-derived CO_2 per year [6,7]. In a context where greenhouse gas emission must be urgently reduced [8–10] and a transition from fossil fuels to renewable energy sources is necessary, there is a growing need for the development of new methods to lower the environmental impact of NF. Besides fixing nitrogen in a more efficient and ecological way, an important challenge to overcome concerns the decentralization of the production in order to reduce the cost and environmental impact of transportation. For this purpose, NF facilities which can be settled locally must be developed.

In the last few years, a lot of attention has been paid to plasmas, which exhibit a great potential for NF[11–14]. While thermal and non-thermal plasmas can be used for NF, only non-thermal plasmas can reach a better energy efficiency (2.5 times more theoretically) than the Haber-Bosch process. Various non-thermal plasma sources can be utilized for NF as e.g. dielectric barrier discharges (DBDs)[15–17], DC/pulsed plasmas-liquid systems [18–20], spark-like plasmas[21,22], gliding arc discharges[23–25], inductively coupled RF (IC-RF)[26] or microwave plasmas[27,28]. In view of applications, efforts must be made to study different types of plasma

reactors in order to obtain an in-depth and global understanding of NF by plasma. For this purpose, the influence of reactor parameters (pressure, gas composition, power…) and reactors engineering aspects (geometry, materials…) on plasma properties and plasma chemistry shall be studied [29]. Moreover, in order to compete with the Haber-Bosch process, the development of plasma systems for NF which are easy to implement and at low cost is going to be one the critical point to consider.

This contribution focuses on NF using an atmospheric-pressure needle-water DC microplasma system operated in N_2/O_2 gas mixtures. The advantage of this simple plasma set-up is the facile operation over a water tank, requiring only a high voltage generator and leading to the dissolution of nitrogen compounds formed in the plasma into the water. Previous studies showed that water treated with various N_2/O_2 plasmas contains stable secondary species such as hydrogen peroxide (H_2O_2), nitrites (NO_2^-) or nitrates (NO_3^-) [19,30–36]. Moreover, it is reported that this type of plasma has a relatively low electron temperature (1-2eV) [37], which allows the vibrational excitation of N_2 through inelastic collisions with electrons. This could favor the efficient dissociation of N_2 molecules and thus allow an energy efficient synthesis process. However, the lack of understanding about the synergistic effect of highly complex gas phase and aqueous phase chemistry does not allow to efficiently and selectively synthesize valuable nitrogen compounds. For example, the synthesis of nitrates by plasma usually leads to the simultaneous formation of nitrites, which are toxic, cannot be absorbed by plants and have therefore little interest[38–40].

This study is aimed to find experimental conditions favorable for the efficient production of nitrates with a reduced formation of nitrites, understand the main mechanisms involved in their formation and discuss possible developments in view of applications, bringing a new insight into plasma-water interactions through a new approach oriented towards NF. Plasma properties are investigated using optical emission spectroscopy (OES) while the activated water is analyzed by ionic chromatography and UV-Visible spectrophotometry. The influence of gas composition (O_2/O_2+N_2, a critical parameter[41,42]) upon nitrites, nitrates and H_2O_2 production is studied in two different configurations: with a water anode and a water cathode. The influence of basic process parameters such as the initial water volume upon nitrites/nitrates formation is also investigated. Gas phase and aqueous phase reaction mechanisms are discussed and ideas for the process improvement/optimization are presented.

Experimental set-up

An atmospheric DC microplasma is ignited between a stainless steel capillary tube (0.2 mm of inner diameter) and an aqueous solution of 1 mM of NaCl (VWR Chemical, CAS 54-21-7) using three beakers of different volumes allowing three different initial water volumes for the process: 6 ml, 27 ml and 50 ml. The plasma is ignited at atmospheric pressure in a closed vessel where a gas flow is constantly running in order to control the atmosphere. The gap between the needle and the water is maintained at 0.7 ± 0.1 mm during the operation (considering the dip induced by the discharge on the water surface). Gas mixtures of different compositions based on N_2 and O_2 (Air liquid, N28 nitrogen and Alphagaz1 oxygen) are injected in the reactor at a fixed total flow of 1 slm. The ratio N_2/O_2 is varied from pure N_2 to gas mixtures having 20, 40, 60 and 80% of O_2 and pure O_2. In order to make the electrical contact to the (conductive) water, a counter electrode of platinum (Pt, Sigma-Aldrich CAS 7440-06-4) is immersed in the solution. The negative high voltage is supplied by a Technix DC generator (5kV) and is either applied to the needle (water anode) or to the platinum counter-electrode (water cathode).

Prior to experiments, the reactor is systematically pumped down to 50 torr and brought back to atmospheric pressure twice by injecting the desired gas mixture. The water+NaCl solution is subsequently injected through a septum to the beaker inside the chamber in order to avoid vacuum evaporation and control the initial humidity level inside the vessel. The plasma is operated by applying 2.3kV to the system with the DC generator. A ballast resistor of 150 kΩ is used to limit the current delivered to the system (see Figure 1), which reaches 10mA in these conditions. Considering the electrical resistance of the different components of the system (evaluated experimentally), the voltage division results in a potential difference of 730V between the needle and the water surface.

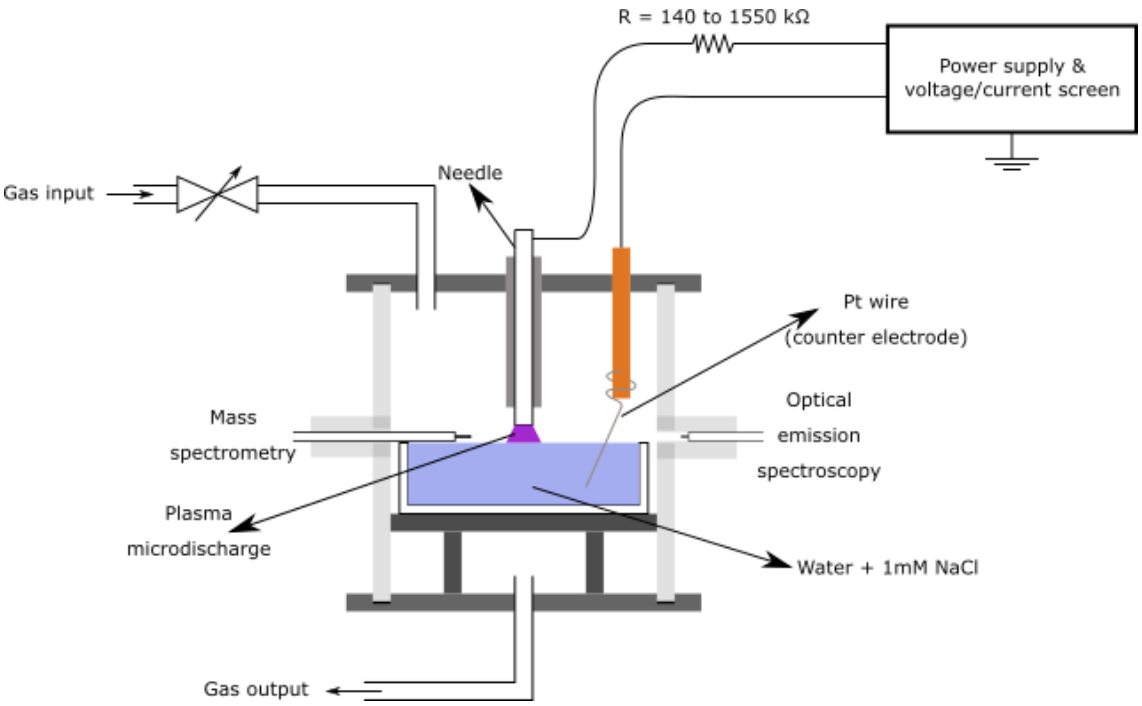

Figure 1: Schematic of the atmospheric pressure DC microplasma experimental set-up.

The solution is analyzed by ionic chromatography using a 930 compact IC flex from Thermo Scientific with a DionexIonPac AG9-HC guard column and a DionexIonPac AS9-HC Analytical column. A solution of 9 mM of Na_2CO_3 (pH = 10,9) is used as an eluant. The conductivity of each species is measured. The measurements are performed at a temperature of 30°C with a volume of 10 µl.

The determination of the H_2O_2 amount in the solution treated by plasma is based on the formation of a complex with titanium oxide which absorbs at 410 nm. The solution is subsequently characterized by UV-vis absorbance spectroscopy using a VWR UV-3100PC spectrometer. All measurements are carried out with 1 cm path length quartz cuvette. The background spectra are collected and subtracted from a solution of $TiOSO_4.xH_2O+H_2SO_4$ (7,39 g/L, Alfa Aesar CAS 13825-74-6).

The pH of the solution is measured with a HI 2209 pH meter from Hanna Instruments with a micro pH-electrode N 5800 BNC from SI Analytics.

Plasmas are analyzed by means of optical emission spectrometry (OES) using an absolutely calibrated Andor Technology SR-500i-D2-R spectrometer and an Andor DU420 CCD camera with an opened electrode (OE). Each optical emission spectrum is acquired using a 1800 grooves/mm grating for overviews (resolution of 0.02nm), and a 2400 grooves/mm grating for

spectra fitting (resolution of 0.0176nm). Each step of the scan averages 4 acquisitions of 3 seconds (full vertical binning). An entrance slit of 160µm is employed in the measurements. The emission spectra are used for the estimation of the rotational and vibrational temperatures of N_2, through the fitting of the N_2 ($C^3\Pi_u \rightarrow B^3\Pi_g$) emission bands. The gas temperature is subsequently calculated by the approximation $T_g = T_{rot}$ and ranges from 1400K to 1800K.
No results of mass spectrometry (shown on Figure 1) are reported in this manuscript since it is unsuitable for the analysis of the species of interest studied in this contribution, i.e. short-lived and/or highly soluble species and radicals. Images of the discharges were obtained using a Nova S6 high-speed camera from Photron, providing a spatial resolution of 838dpi.

Results and discussion

Influence of the oxygen content on plasma properties with a water anode

In this section, microplasmas are ignited by applying the 2.3kV negative high voltage to the needle (730V between the needle and the water surface). The experiments are performed using three beakers of different initial volumes (6, 27 and 50ml) and the amount of oxygen in the gas mixture is varied while keeping a total gas flow of 1slm. Considering the complexity of studying short lived species and soluble compounds in a closed vessel, plasmas are here mainly characterized using OES.

Undoubtedly, the N_2/O_2 ratio in the initial gas mixture impacts greatly the properties of the discharge. One good example concerns the electron density, which is lowered with increasing proportions of oxygen, due to the formation of negative ions by electron attachment [43]. This is illustrated by the plasma light emission which varies as a function of the oxygen content in the gas mixture (Figure 2(a)). The global light emission intensity –mainly coming from the second positive system of N_2 and O atoms emission lines– decreases along with the increase of the oxygen content in the gas mixture. This is most likely due, at least partly, to the decrease of the electron density in the plasma. The consequence for the process, in addition to a different chemistry set, is a reduced electron impact excitation of the different species present in the discharge (in particular N_2) which impacts the overall NF.

A precise estimation of the electron density is difficult to perform in this system since the H_β emission line cannot be observed by OES and the H_α line is barely visible in the noise level of pure N_2 plasma spectra. Nonetheless, for gas mixtures similar to air (i.e. with 20% O_2), a

range can be at least estimated based on the electrical parameters of the discharge such as the electric field E, the current density j and the electron mobility in air μ_e using the relation [44,45]:

$$n_e = \frac{j}{E * \mu_e * e}$$

Here e is the electron charge. The electron mobility μ_e ($cm^2/V/s$) can be determined as a function of the gas temperature T (K), assuming that the following equation is linear:

$$(\mu_e * p)_T = \frac{T}{T_0}(\mu_e * p)_{T_0}$$

$$(\mu_e * p)_{T_0} = 0.45 * 10^6\, cm^2\, Torr / V\, s$$

The pressure p equals to 760torr, and T_0 is the room temperature i.e. 25°C. Based on imaging experiments of the discharge, the microplasma can be modeled as a cylinder of 0.75mm diameter. Therefore a current density of 2.26 A/cm^2 can be estimated by dividing the current flowing through the plasma by the section area of this cylinder. Considering the voltage of 730V between the needle and the water resulting in a voltage of 500V in the positive column (after subtraction of the cathode fall[46,47]) and that the corresponding gap with the water dip is 0.7mm ± 0.1mm, the resulting electric field is 6800V/cm ± 800V/cm. By using these parameters, the calculated electron density decreases with increasing temperatures, from $3.4*10^{12}$ ($\pm 4*10^{11}$) to $1*10^{12}$ ($\pm 1.2*10^{11}$) cm^{-3} between ambient temperature and 1000K, and from $1*10^{12}$ ($\pm 1.2*10^{11}$) to $5.1*10^{11}$ ($\pm 6.10^{10}$) cm^{-3} between 1000K and 2000K (typical temperature range for this type of discharge). It can thus be assumed that the order of magnitude for the electron density is 10^{11} cm^{-3} for all conditions studied with a water anode, with a decrease along with the increase of the oxygen content. The uncertainty regarding the exact value of the electric field in the positive column region or the modification of the electron mobility for the different electronegative gas mixtures (in particular considering the water evaporation following the plasma ignition) are possible sources of error which entangle the accurate estimation of the electron density. The slightly different cross section of the plasma along the discharge axis may also be considered.

The fraction of oxygen in the initial gas mixture which impacts the electron density, the different mix of molecular species and leads to the formation of negative ions (resulting in different transport properties) is expected to have a huge influence on NF. The first clue concerns the formation of NO in the gas phase, which is the first step of NF. The decrease of the NO-γ ($A\ ^2\Sigma^+ \rightarrow X\ ^2\Pi$) light emission with increasing oxygen fractions (Figure 2(b)) may

indicate a lower yield for the overall NO_x production. This is based on the fact that not only the total light emission of these bands decreases, but also the ratio of these bands to the N_2 ($C^3\Pi_u \rightarrow B^3\Pi_g$) bands (see Figure 3(a)). The intensity of the NO-γ emission system is systematically maximum for pure N_2 discharges.

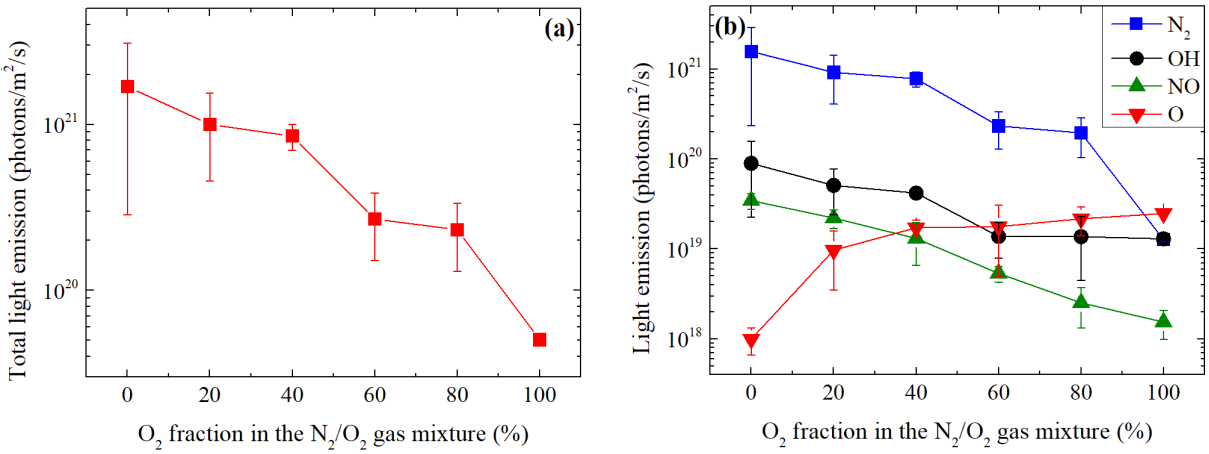

Figure 2: (a) Total light emission (200 to 900nm) and (b) light emission of the main radiative species of the DC microplasma as a function of O_2 fraction in the N_2/O_2 gas mixture (atmospheric pressure, total gas flow = 1slm). The light emission is calculated from the integration of the absolutely calibrated OES spectra. The plasma is operated with 730V between the electrodes (water anode, separated by 0.7mm). The current intensity is 10mA.

Although OES measurements only concern the plasma region and cannot be used for a quantitative analysis of NO, this result at least gives an indication about favorable experimental conditions for its formation and suggests that the oxygen source for the formation of NO in the discharge can be questioned. Indeed, no oxygen atom could be detected by OES in N_2 discharges while the presence of a significant amount of NO is identified in the plasma region. The intensity of the OH ($A^2\Sigma^+ \rightarrow X^2\Pi$) emission line at 306.3nm evolves similarly as the NO ($A\ ^2\Sigma^+ \rightarrow X\ ^2\Pi$) bands and is also maximum in the case of pure N_2 microplasmas. It is thus likely –at least for low oxygen contents- that one of the main mechanisms (maybe the dominant) for NO formation is the "extended Zeldovich mechanism" (R4) between N atoms and OH radicals, and cannot be restricted to reactions between N/N_2 and O/O_2 (reactions R1 to R3). In addition, considering the plasma-water configuration, the formation of HO_2 in the discharge and its potential involvement in NO

production (R5) may be considered as well[48]. However because HO_2 and OH are intermediary species, it is difficult to know precisely about the kinetics of such reactions.

$N_2(X, v) + O \rightarrow NO + N$		(R1)	11,23
$N + O_2 \rightarrow NO + O$	$k = 1.6 * 10^{-14} e^{\frac{-3150}{Tg}} [cm^3.s^{-1}]$	(R2)	11,23,27
$N + O + M \rightarrow NO + M$	$k = 6.3 * 10^{-45} * e^{\frac{140}{Tg}} [cm^3.s^{-1}]$	(R3)	49
$N + OH \rightarrow NO + H$	$k = 4.7 * 10^{-11} [cm^3.s^{-1}]$	(R4)	20,50
$N + HO_2 \rightarrow NO + OH$	$k = 2.2 * 10^{-11} [cm^3.s^{-1}]$	(R5)	51

Another point to consider is the presence of the NH ($A\ ^3\Pi \rightarrow X\ ^3\Sigma$) emission line at 336nm, visible on the OES spectrum when the discharge is operated in pure N_2 (it cannot be detected when O_2 is added to the gas mixture). It is not perfectly clear how NH is formed but it could be through reactions between H_2O and $N(^2D)$ metastables (R6) or between HO_2 and N atoms (R7). Thus NH radicals might contribute to the formation of NO (R8) in pure N_2 microplasmas, and could explain partly the higher level of NO in the discharge in these conditions.

$H_2O + N(^2D) \rightarrow OH + NH$	$k = 2.5 * 10^{-10} [cm^3.s^{-1}]$	(R6)	51
$HO_2 + N \rightarrow NH + O_2$	$k = 1.7\ 10^{-13} [cm^3.s^{-1}]$	(R7)	
$NH + OH \rightarrow NO + H_2$	$k = 8 * 10^{-11} [cm^3.s^{-1}]$	(R8)	52

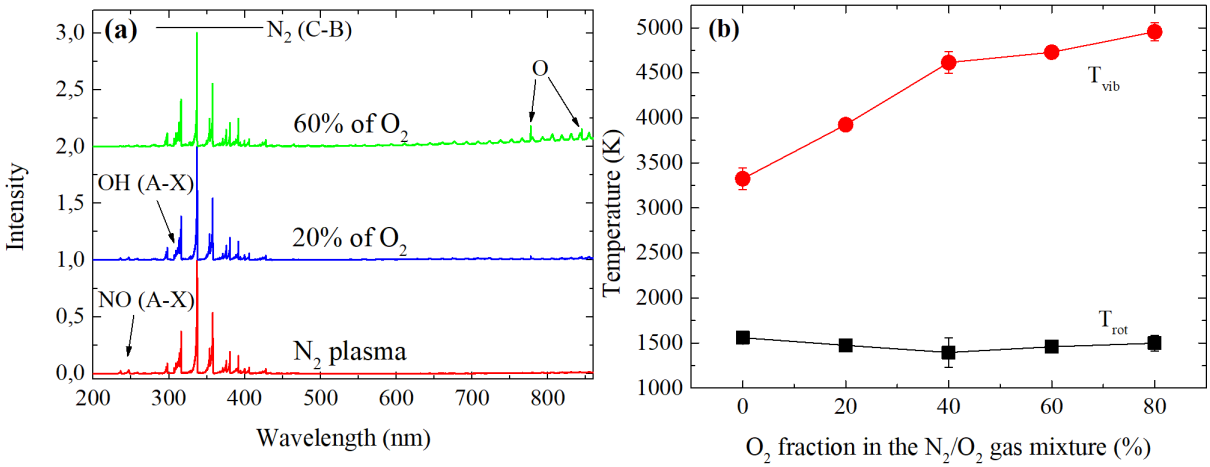

Figure 3: (a) Optical emission spectra normalized to the highest peak (337nm) of the DC N_2/O_2 microplasmas (see Figure 7(a) for a more detailed picture of the region of interest) and (b) rotational and vibrational temperature of the discharges as a function of the oxygen fraction in the gas mixture. The negative high voltage of 730V (2.3kV supplied by the generator) is applied to the needle (water anode, 0.7mm from the water surface), the current is set to 10mA.

Ozone formation and contribution to NO_x formation is not considered here because of the elevated gas temperature of the plasma. It is indeed known that in high pressure plasmas, the rate coefficients for the production and destruction of O_3 are highly dependent on the gas temperature [53,54]. By evaluating the rotational temperature of N_2 (C-B), an estimation of the gas temperature using optical emission spectroscopy can be done and is systematically above 1000K, which is not favorable to ozone production.

The approximation $T_g = T_{rot}$ (N_2) is a common method to estimate the gas temperature of a non-thermal plasma by fitting the N_2 ($C^3\Pi_u \rightarrow B^3\Pi_g$) emission bands [55–58]. Yet, considering the complex mixture of several molecular species studied here, it is difficult to assume that the rotational temperature of N_2(C-B) is systematically in equilibrium with the translational energy since slight discrepancies can be found between T_{rot} from different ro-vibrational bands, especially when the oxygen proportion is increased in the gas mixture. This is usually caused by a non-Boltzmann distribution of the rotational population of N_2(C) [56,57]. Here T_{rot} is obtained by fitting simultaneously the ro-vibrational bands between 340nm and 385nm together i.e. the 0-1, 1-2, 2-3, 0-2, 1-3, 2-4 and 3-5 bands, using the software MassiveOES[59,60]. The T_{rot} obtained ranges between approximately 1450 and 1550 K (Figure 3(b)), which corresponds to the usual gas temperature expected for this type of plasma [37]. In these conditions, it can be assumed that the gas temperature belongs to a similar range.

The vibrational temperature of N_2 is estimated using the same method and ranges from 3500K to 5000K. It increases along with the increase of the oxygen content in the gas mixture. It is known that an elevated gas temperature enhances the vibrational-translational energy transfers and depopulate the high-energy vibrational levels of N_2 [23]. It is yet expected that a higher vibrational excitation of nitrogen molecules leads to an improved dissociation of N_2 and thus to favorable conditions regarding NF.

Nitrites/nitrates formation in the liquid phase with a water anode

The formation of NO in the gas phase is the first step of NF by plasma, but it is not an end in itself and the further oxidation and/or collection of this compound is necessary. One major advantage of plasma-water systems is that the different NO_y (NO, NO_2, HNO_2…) formed in the discharge can be simply and directly dissolved in the water and contribute to the formation of stables species of interest i.e. nitrites and nitrates. However, because of the low solubility of NO (Henry's law constant = $1.9*10^{-5}$ $mol.m^{-3}.Pa^{-1}$)[61], a significant proportion of this compound is lost in the exhaust gases. The consequence is a decrease of the energy efficiency of the process and the emission of a harmful gas to the environment. Therefore, the oxidation of NO to other compounds with a higher solubility as e.g. NO_2, HNO_2 or HNO_3 has a high importance for the development of a NF process allowing the direct collection of all nitrogen compounds in the activated water.

In the following experiment the amount of NO_2^- and NO_3^- in the activated water following a DC microplasma treatment is measured by means of ionic chromatography as a function of the oxygen fraction in the gas mixture. For each condition the plasma is operated for 12min by applying 2.3kV to the system (water anode, 730V between the water and the needle) providing a current of 10mA. Ionic chromatography is performed directly after the end of the plasma treatment. The data are subsequently processed in order to assess the proportions of HNO_2 to NO_2^- based on the pKa of the reaction $HNO_2 + H_2O \rightarrow NO_2^- + H_3O^+$, using the concentration of NO_2^- measured by ionic chromatography and the measured solution pH (see Figure 4 (a), (b) and (c)). It should be noted that this only concerns the composition of the activated water at the end of plasma treatment and does not consider its further evolution.

As expected, with a higher fraction of oxygen in the initial gas mixture, proportionally more nitrates than nitrites are measured in the activated water. This is presumably due to different mechanisms in the gas phase involving O atoms or O_2 molecules which causes the oxidation of NO to other NO_x as e.g. NO_2 (R9). At the same time the highest content of $NO_2^- + NO_3^-$ in the activated water is found for an oxygen fraction ranging from 20% to 60%, with a maximum value systematically found in the case of a gas mixture having 20% of oxygen. This is very valuable for future applications where atmospheric air could be used as a precursor. When pure N_2 discharges are operated, the amount of nitrogen compounds detected in the water is relatively lower while the light emission of the NO ($A\ ^2\Sigma^+ \rightarrow X\ ^2\Pi$) bands measured by OES is maximum. This result highlights that the further oxidation of NO in the

gas phase –here most probably through reactions with O atoms- contributes to the improvement of the system energy efficiency through the direct dissolution of NO_x with a higher solubility in the water (Henry's law constant = $1.2*10^{-4}$ $mol.m^{-3}.Pa^{-1}$ for NO_2 and $3.8*10^{-4}$ $mol.m^{-3}.Pa^{-1}$ for NO_3)[61]. H_2O_2 could be measured in all conditions studied (Figure 4(d)), but no clear tendency for its formation is visible as a function of the oxygen content or the initial water volume.

$$NO + O \rightarrow NO_2 \qquad k = 3*10^{-11} ¿] \text{ (R9)} \quad [20]$$

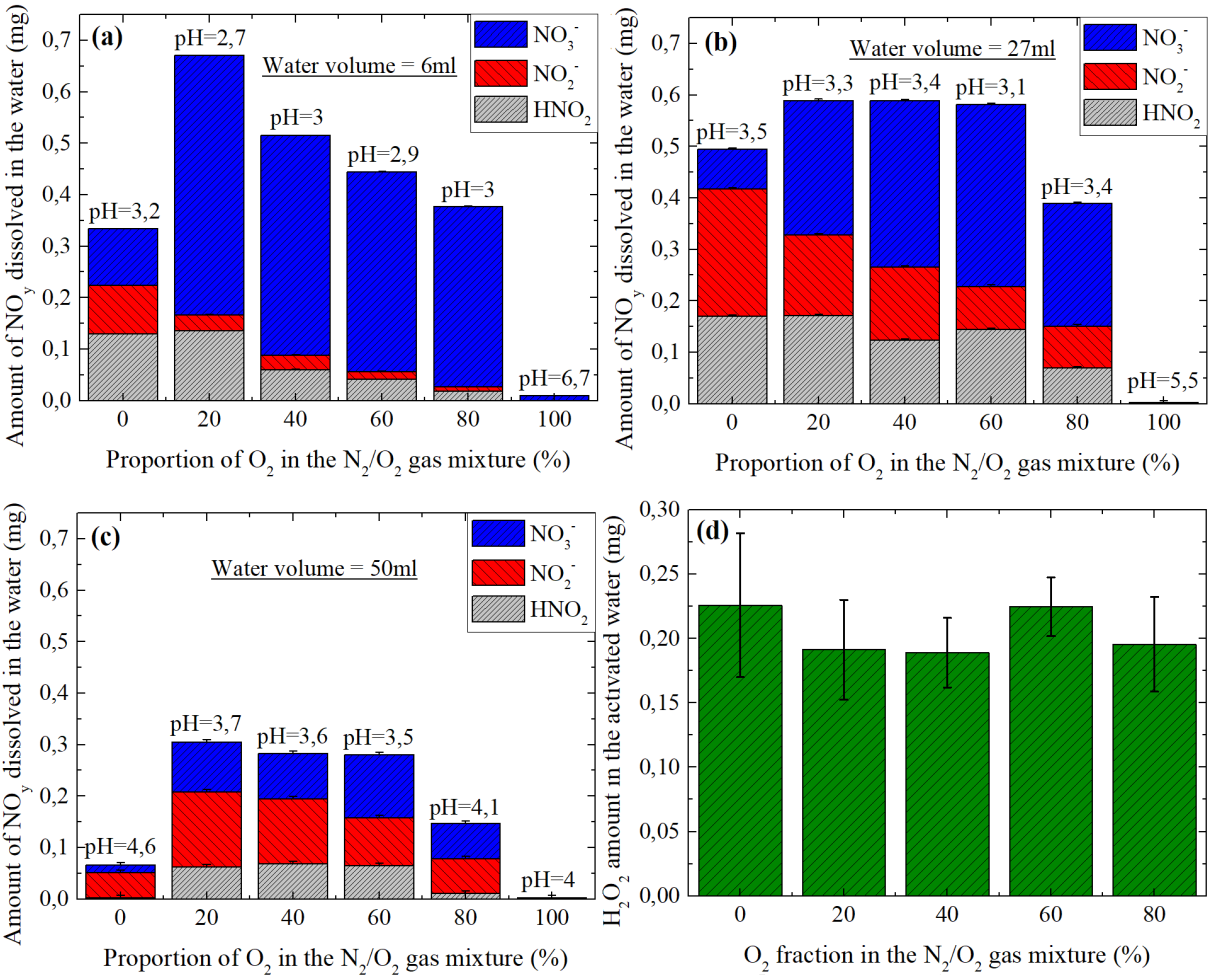

Figure 4: NO_y measured in the activated water by ionic chromatography following the 12min DC microplasma treatment for different proportions of O_2 in the gas mixture and for water volumes of 6ml (a), 27ml (b) and 50ml (c) and (d) the corresponding H_2O_2 concentration in the solution. The ionic chromatography measurements are performed directly after the plasma is switched off. The discharge is ignited at atmospheric pressure by applying a negative voltage of 730V to the needle (water anode, 2.3kV on the generator, 0.7mm between the needle and the water) and a current of 10mA for 12min. The total gas flow is fixed to 1slm.

Surprisingly, the global amount of NO_y present in the activated water is globally higher when the process is performed using smaller initial water volumes (Figure 4 (a), (b) and (c)). Furthermore, the proportion of NO_3^- to (NO_2^- + HNO_2) increases when experiments are performed using small water volumes and NO_3^- is even the dominant nitrogen-containing compound for most of the experiments performed with 6ml of water. Although such differences when varying the water volume during the treatment are not expected, a temperature measurement using a thermocouple indicates that the water temperature increases up to 60°C when a plasma is operated over 6ml of water but remains close to room temperature when the water volume is 50ml. The increase of the water temperature causes a lower dissolution of gases (lower Henry's law constant), but it also causes a higher water vapor pressure resulting in more OH radicals in the gas phase and speeds up the dissolution as well as the reactions kinetics in the aqueous phase. Therefore, it can be assumed that when the water temperature increases, the solution will be more rapidly saturated in NO which will be converted faster, leading eventually to an increase of the amount of NO_y found in the solution as well as a larger proportion of NO_3^- due to a higher reaction kinetics for its formation.

Nitrites conversion following the plasma treatment

It is known that the concentration of NO_2^-, NO_3^- and H_2O_2 evolves as a function of time in the activated water following a plasma treatment[62]. The two main reactions involved concern the conversion of nitrites: either a disproportionation of NO_2^- can occur if the pH of the solution is below 3.5 (R10), or NO_2^- can react with H_2O_2 to form NO_3^- and H_2O (R11).

$$3NO_{2\,(aq)}^- + 2H_{(aq)}^+ \rightarrow 2NO_{(aq)} + NO_{3\,(aq)}^- + H_2O_{(l)} \qquad \text{(R10)}$$

$$NO_{2\,(aq)}^- + H_2O_{2(aq)} \rightarrow NO_{3\,(aq)}^- + H_2O_{(l)} \qquad \text{(R11)}$$

Regarding the stoichiometry of (R10), the amount of NO_y in the solution should decrease after the plasma treatment. Although ionic chromatography measurements performed as a function of time following the treatment shows as expected a decrease of the NO_2^-/HNO_2 content and an increase of the amount of NO_3^-, no significant decrease of the global amount of NO_y could be highlighted. Consequently, (R11) is most likely the dominant nitrite conversion reaction involved in the transformation of the activated water following the treatment, which allows to avoid the loss of nitrogen compounds synthesized in this process to the air. However, nitrites are toxic and cannot be absorbed by plants [38–40], and the delay to convert the nitrites to nitrates

in the solution is unsuitable for applications, which stresses the need to synthesize nitrates without residual nitrites.

Nitrogen fixation with a water cathode

If the (negative) high voltage is now applied to the counter electrode instead of the needle (water cathode), the plasma exhibits a different behavior. Because of the asymmetric nature of DC discharges, the shape of the plasma appears to be broader and bell-shaped as shown on Figure 5, leading to a larger plasma-water interface. It is known that having cathode sheath on the water surface in DC plasmas causes a strong water evaporation due to the ion bombardment on the water surface and a strong local heating, especially considering the higher cathode fall for a water cathode compared to a stainless steel cathode[37,46,63]. Here it is assumed that the relative humidity in the gas mixture reaches 100% within only a few minutes of treatment (730V, 10mA) according to the intense condensation inside the reactor. A decrease of the water volume by 1-2 ml after 12min of plasma treatment –which is not measurable in the water anode configuration– is systematically observed.

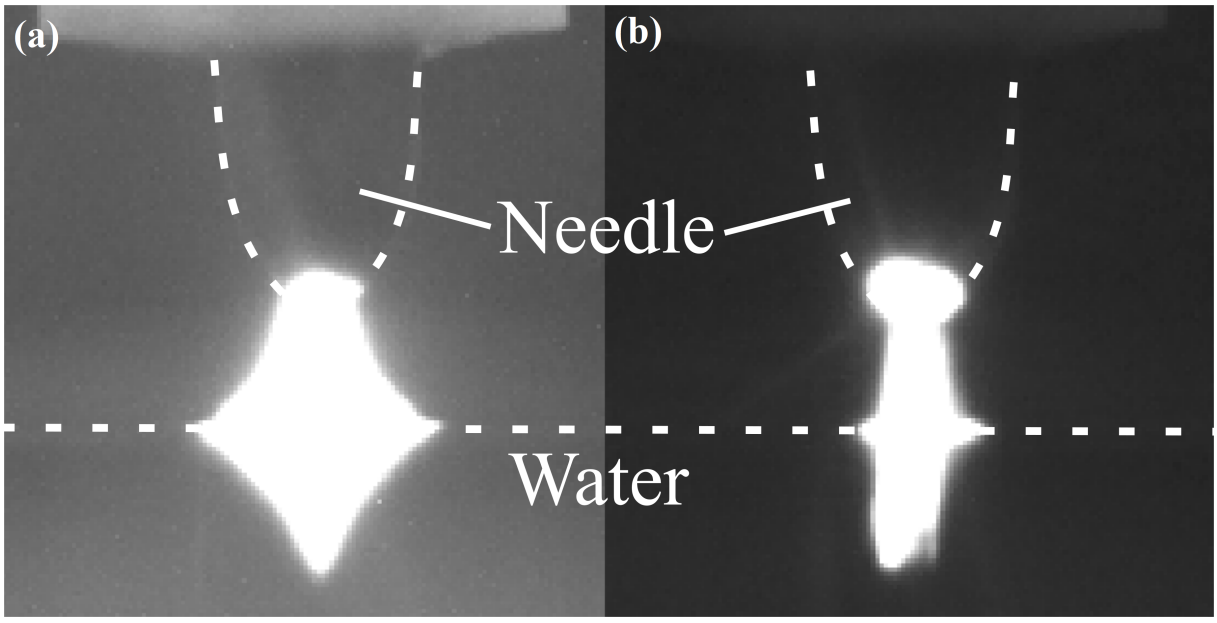

Figure 5: Picture of the plasma when the negative high voltage is applied to (a) the water (water cathode) and (b) the needle (water anode). The plasma is ignited using 730V (2.3kV provided by the generator) and 10mA of current over a water tank of 27ml. The gas mixture has 60% of N_2 and 40% of O_2 (total flow = 1lpm).

In this configuration, the enhanced plasma-induced water heating, different plasma properties and plasma-liquid interactions impact nitrites/nitrates formation in the water during the process. As presented on Figure 6 (a), (b) and (c), NO_3^- is the only nitrogen anion detected by ionic chromatography in the activated water following the plasma treatment for all gas mixtures studied (from 0 to 80% O_2) and using the three different initial water volumes (6, 27 and 50ml), with a globally much higher energy efficiency. Under the same experimental conditions, up to 2mg of nitrates are produced in the best case here while only 0.67 mg of NO_y (NO_3^- + NO_2^- + HNO_2) are produced in the best case in the water anode configuration. According to OES measurements (see Figure 7(a)) the density of OH radicals in the plasma is substantially higher here for all experimental conditions which is a direct consequence of the strong plasma-water interaction. The initial NO formation through the extended Zeldovich mechanism can therefore be enhanced by this higher density of OH radicals in the gas phase (R4). Moreover, the two and three body reactions (R12 to R15) between OH and NO/NO_2, leading to the formation of the highly soluble HNO_2 and HNO_3 may be one of the reasons for the higher energy efficiency. At the same time the amount of H_2O_2 produced in the plasma and dissolved in the water (Figure 6(d)) is much higher than in the water anode configuration, which enhances the conversion of nitrites to nitrates in the liquid phase (R11) during and after the treatment, and may explain why NO_3^- is the only nitrogen anion found in the solution. This is confirmed by the slightly lower amount of H_2O_2 in the solution (Figure 6(d)) when the amount of NO_3^- measured in the solution is maximum (i.e. for pure N_2 discharges). The higher amount of NO_3^- produced with increasing initial water volumes (maximum for 50ml) may be explained by the solution capability to dissolve more NO_x such as NO and NO_2.

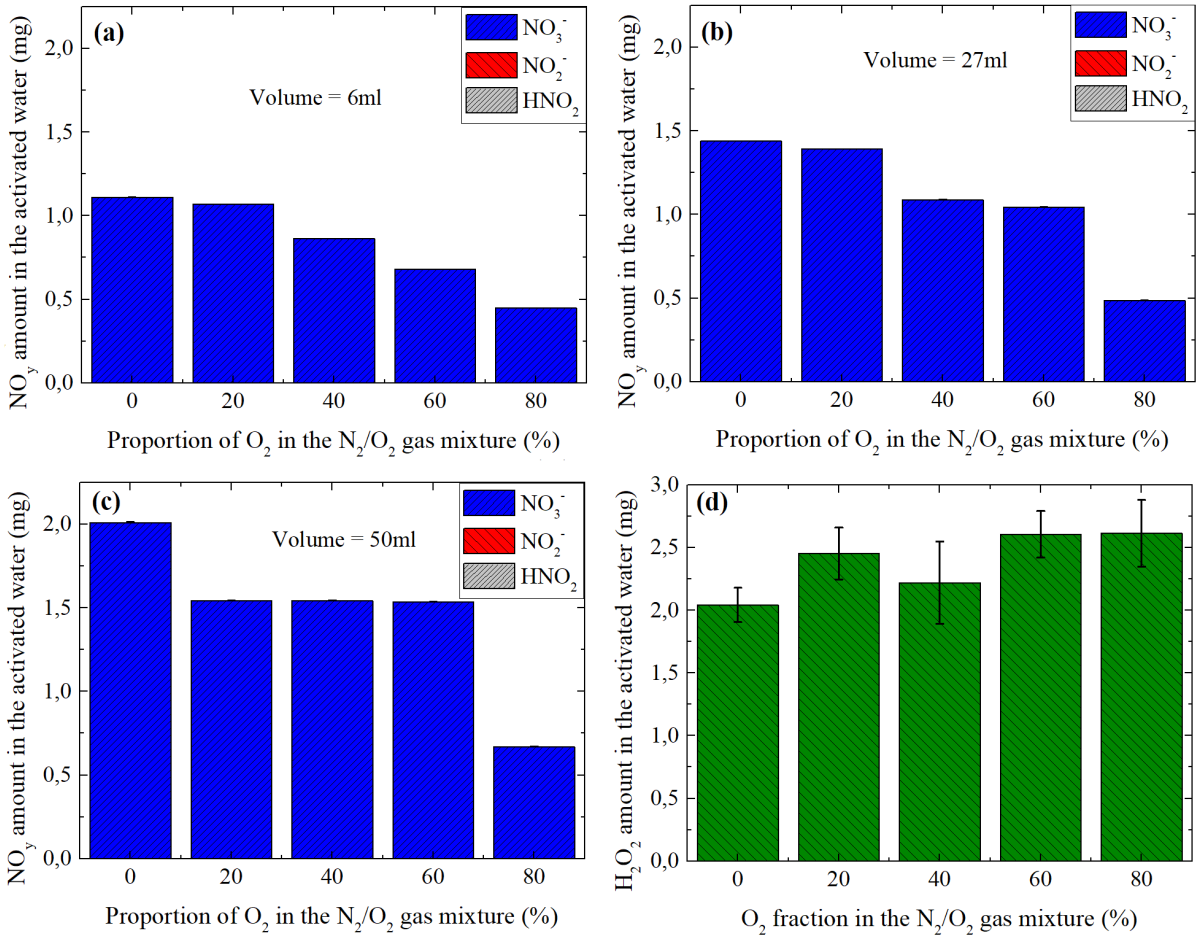

Figure 6: NO_y measured in the activated water by ionic chromatography following the 12min DC microplasma treatment for different proportions of O_2 in the gas mixture and for water volumes of 6ml (a), 27ml (b) and 50ml (c) and (d) the corresponding H_2O_2 concentration in the solution. The measurements are performed directly after the plasma is switched off. The discharge is ignited at atmospheric pressure by applying a negative voltage of 730V to the water (water cathode, 2.3kV on the generator, 0.7mm between the needle and the water) and a current of 10mA. The total gas flow is fixed to 1slm.

Because NO_3^-/HNO_3 are the only NO_y found in solution following the plasma treatment, the global improvement of the system energy efficiency can be attributed to an enhanced conversion of NO into other NO_y during the process in both the gas phase and aqueous phase and reduced loss to the gas exhaust in the continuous flow configuration. However, it is important to question if the different plasma properties can impact the efficiency of N_2 dissociation in the gas phase and also play a role in the improvement of the system energy efficiency.

$OH + NO \rightarrow HNO_2$ (R12) [64]

$OH + NO_2 \rightarrow HNO_3$ (R13) [64]

$OH + NO + M \rightarrow HNO_2 + M$ (R14) [65]

$OH + NO_2 + M \rightarrow HNO_3 + M$ (R15) [65]

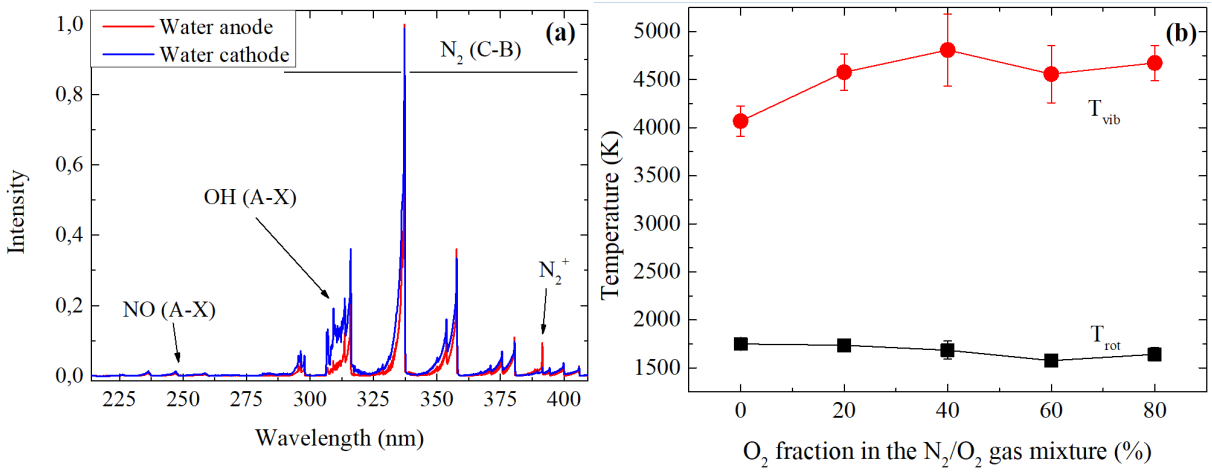

Figure 7: (a) comparison of N_2 microplasmas OES spectra normalized to their highest peak (337nm) in the water cathode and water anode configuration (water tank = 50ml) and (b) rotational and vibrational temperature of plasmas ignited with a water cathode for different oxygen fractions. The plasmas are operated with 730V, 10mA and with a water-needle distance of 0.7mm.

Considering the higher plasma volume under similar experimental conditions (in particular with the same current), and the lower secondary electron emission caused by ion bombardment on the water compared to stainless steel[66], the electron density might be globally lower in the water cathode configuration. However, the higher gas temperature (Figure 7(b)) and the stronger cathode fall on the water surface resulting in a lower electric field in the positive column counterbalance this effect. It is thus difficult to conclude that there is a significant difference in the electron density between the water anode and the water cathode configurations. The intensity of the N_2^+ emission peak at 391nm decreases significantly when the water surface is the cathode (Figure 7(a)). In a similar set-up, Wilson et al. argued that this could be due either to a decrease of N_2^+ concentration or to an increase of the electronic excitation temperature[63]. In the present case, the ion bombardment on the water surface is probably causing N_2^+ ions quenching and thus a decrease of its concentration in the

plasma. Regarding the similarities for the rest of the OES spectra in comparison to the water anode configuration, a significant modification of the electronic excitation temperature cannot be assumed, but a modification of the electron energy distribution function (EEDF) involving proportionally less high-energy electrons –necessary for the emission of N_2^+- is not ruled out[45]. The vibrational temperature of N_2, which is globally slightly higher in the present configuration, especially at low oxygen fractions (ranging from 4450 to 4850K in average), seems to confirm this point. This higher vibrational excitation which is favorable for the efficient dissociation of N_2 in the plasma might indeed be caused by a shift of the EEDF towards lower energies due to a lower reduced electric field, which could contribute to the better energy efficiency of the process.

Process improvement

Although the experimental set-up presented here is aimed for fundamental study and has not been optimized, it could produce up to 2mg of nitrates in the treated water for a total energy efficiency of 513.4MJ/mol for NO_3^-. However, about two thirds of the energy spent is lost to heating the ballast resistor. If one considers only the energy input to the plasma, the energy efficiency increases to 167.4MJ/mol. Despite the fact that this is still far from reaching the energy efficiency of the Haber-Bosch process, nitrates are produced directly without requiring the Ostwald process. This significant advantage in a very easy to implement system is promising for future applications, and seeing such a technology used in a near future for industrial NF seems realistic. However, in order to reach to this goal, further improvement to efficiently convert and collect all the NO_x formed in the discharge (in particular NO) is necessary. A proper understanding of the vibrational kinetics of N_2 for its efficient dissociation is also missing.

As presented previously, the "extended Zeldovich mechanism" between N atoms and OH radicals is thought to be the dominant mechanism for the initial production of NO in the gas phase. However, in order to improve the energy efficiency of the process, the reaction (R1) which activation energy is lowered by the vibrational excitation of N_2 should be enhanced. The main difficulty is to understand the vibrational excitation mechanisms and collisional energy transfer between molecules in the plasma. According to what was published in [28], vibrational-vibrational (V-V) relaxation which allows to shift the vibrational distribution function of N_2 towards high-energy levels should be enhanced while vibrational-translational

(V-T) relaxation, which contributes to the loss of vibrational excitation to heating the gas should be avoided. This is especially important at elevated gas temperatures [23]. As suggested in [28,67] for different plasma systems, one possibility to overcome this problem would be to use pulsed plasmas, in order to allow the gas to cool down between each pulse and benefit from the different time scales of the collisional mechanisms.

In any cases, in spite of a growing literature in the field of atmospheric pressure plasmas interacting with water, providing a rather good knowledge of these discharges, joined experimental-computational studies are lacking. This contribution, as many others, illustrates how challenging the experimental study of atmospheric pressure discharges is. In the field of NF by plasma, it will be necessary to perform such joined-researches in the future to understand better the chemical kinetics occurring in both the gas phase and liquid phase. In addition, the simulation of N_2 vibrational kinetics supported by experimental data would likely be necessary to improve the energy efficiency of plasma-water NF systems.

Conclusion

The potential of DC needle-water microplasmas for NF has been presented. Experiments highlighted that the extended Zeldovich mechanism between N atoms and OH radicals is most likely the dominant mechanism for the initial NO formation in the gas phase. The energy efficiency of NF and the ratio of nitrites to nitrates dissolved in the water during the treatment were highly dependent on many parameters, one of which is the initial water volume. For the smaller volumes, water heating induced by the discharge could enhance nitrogen compounds formation in the liquid phase while reducing the proportion of nitrites in the solution.

It was possible to synthesize nitrates without any residual nitrites dissolved in the water in a water cathode configuration, which also caused a drastic increase of the energy efficiency of the whole system. The stronger water evaporation, different plasma properties and broader plasma-water interface lead to a much stronger OH radical density in the plasma and H_2O_2 formation in the water, which are involved in an enhanced conversion of the different NO_y into HNO_3/NO_3^- in both the gas phase and aqueous phase.

The selective synthesis of nitrates (i.e. nitrates formation without residual nitrites) has a great potential for applications, but a proper understanding of the vibrational kinetics of N_2 is yet required to optimize the dissociation of this molecule and thus improve the system energy

efficiency towards acceptable values. One possibility could be to investigate the effect of pulsing the discharge to study the time scale of the different collisional mechanisms instead of working with a continuous discharge. Future work will certainly require a joint experimental-computational study for a clearer understanding of reactions and vibrational kinetics in such highly complex plasma-water systems for NF.

Acknowledgment

The authors want to acknowledge the financial support provided by the Belgium Excellence of Science through the NITROPLASM project (EoS 30505023).

References

1 J. N. Galloway, J. D. Aber, J. A. N. W. Erisman, P. Sybil, R. W. Howarth, E. B. Cowling and B. J. Cosby, The Nitrogen Cascade, *Bioscience*, 2003, **53**, 341–356.

2 J. W. Erisman, M. A. Sutton, J. Galloway, Z. Klimont and W. Winiwarter, How a century of ammonia synthesis changed the world, *Nat. Geosci.*, 2008, **1**, 636–639.

3 V. Smil, Global Population and the Nitrogen Cycle Feeding, *Sci. Am.*, 1997, **277**, 76–81.

4 J. N. Galloway, A. R. Townsend, J. W. Erisman, M. Bekunda, Z. Cai, J. R. Freney, L. A. Martinelli, S. P. Seitzinger and M. A. Sutton, Transformation of the Nitrogen Cycle : Recent Trends, Questions, and Potential Solutions, *Science (80-.).*, 2008, **320**, 889–893.

5 J. N. Galloway and E. B. Cowling, Reactive Nitrogen and The World : 200 Years of Change, *Ambio*, 2002, **31**, 64–71.

6 A. Anastasopoulou, S. Butala, J. Lang, V. Hessel and Q. Wang, Life Cycle Assessment of the Nitrogen Fixation Process Assisted by Plasma Technology and Incorporating Renewable Energy, *Ind. Eng. Chem. Res.*, 2016, **55**, 8141–8153.

7 Y. Tanabe and Y. Nishibayashi, Developing more sustainable processes for ammonia synthesis, *Coord. Chem. Rev.*, 2013, **257**, 2551–2564.

8 D. A. Lashof and D. R. Ahujah, Relative contributions of greenhouse gas emissions to global warming, *Lett. to Nat.*, 1990, **344**, 529–531.

9 M. Meinshausen, N. Meinshausen, W. Hare, S. C. B. Raper, K. Frieler, R. Knutti, D. J. Frame and M. R. Allen, Greenhouse-gas emission targets for limiting global warming to 2°C, *Nat. Lett.*, 2009, **458**, 1158–1163.

10 P. M. Cox, R. A. Betts, C. D. Jones and S. A. Spall, Acceleration of global warming due to carbon-cycle feedbacks in a coupled climate model, *Lett. to Nat.*, 2000, **408**, 184–187.

11 N. Cherkasov, A. O. Ibhadon and P. Fitzpatrick, A review of the existing and alternative methods for greener nitrogen fixation, *Chem. Eng. Process. Process Intensif.*, 2015, **90**, 24–33.

12 V. Hessel, G. Cravotto, P. Fitzpatrick, B. S. Patil, J. Lang and W. Bonrath, Industrial applications of plasma, microwave and ultrasound techniques: Nitrogen-fixation and hydrogenation reactions, *Chem. Eng. Process. Process Intensif.*, 2013, **71**, 19–30.

13 V. Hessel, A. Anastasopoulou, Q. Wang, G. Kolb and J. Lang, Energy , catalyst and reactor considerations for (near) -industrial plasma processing and learning for nitrogen-fixation reactions, *Catal. Today*, 2013, **211**, 9–28.

14 S. Li, J. A. Medrano, V. Hessel and F. Gallucci, Recent Progress of Plasma-Assisted Nitrogen Fixation Research: A review, *Processes*, 2018, **6**, 248.

15 B. S. Patil, N. Cherkasov, J. Lang, A. O. Ibhadon, V. Hessel and Q. Wang, Low temperature plasma-catalytic NOx synthesis in a packed DBD reactor : Effect of support materials and supported active metal oxides, *Appl. Catal. B, Environ.*, 2016, **194**, 123–133.

16 S. Simon, C. Bailly, T. Dufour and F. Jud, Plasma-activation of tap water using DBD for agronomy applications : Identification and quantification of long lifetime chemical species and production / consumption mechanisms, *Water Res.*, 2018, **133**, 47–59.

17 F. Girard, V. Bedets, S. Blanc, K. Gazeli, L. Marlin, L. Authier, P. Svarnas, N. Sojic and S. Arbault, Formation of Reactive Nitrogen Species including Peroxynitrite in Physiological Buffer exposed to Cold Atmospheric Plasma, *RSC Adv.*, 2016, **0**, 1–11.

18 H. Zheng, X. Guan, X. Mao, Z. Zhu and C. Yang, Determination of nitrite in water samples using atmospheric pressure glow discharge microplasma emission and chemical vapor generation of NO species, *Anal. Chim. Acta*, 2018, **1001**, 100–105.

19 W. Bian, J. Shi and X. Yin, Nitrogen Fixation Into Water by Pulsed High-Voltage Discharge, *IEEE Trans. Plasma Sci.*, 2009, **37**, 211–218.

20 R. J. Wandell, H. Wang, R. K. M. Bulusu, R. O. Gallan and B. R. Locke, Formation of Nitrogen Oxides by Nanosecond Pulsed Plasma Discharges in Gas – Liquid Reactors, *Plasma Chem. Plasma Process.*, 2019, **39**, 643–666.

21 D. P. Park, K. Davis, S. Gilani, C. Alonzo, D. Dobrynin, G. Friedman, A. Fridman, A. Rabinovich and G. Fridman, Reactive nitrogen species produced in water by non-equilibrium plasma increase plant growth rate and nutritional yield, *Curr. Appl. Phys.*, 2013, **13**, 1–11.

22 M. J. Pavlovich, D. S. Clark and D. B. Graves, Air spark-like plasma source for antimicrobial NOx generation, *J. Phys. D. Appl. Phys.*, 2014, **47**, 505202.

23 A. W. Wang, B. S. Patil, S. Heijkers and A. Bogaerts, Nitrogen Fixation by Gliding Arc Plasma: Better Insight by Chemical Kinetics Moddelling, *ChemSusChem*, 2017, **10**, 2145–2157.

24 B. S. Patil, Plasma Assisted Nitrogen Oxide Production from Air : Using Pulsed Powered Gliding Arc Reactor for a Containerized Plant, *AIChE*, 2018, **64**, 526–537.

25 B. S. Patil, V. Hessel and Q. Wang, Plasma Nitrogen Oxides Synthesis in a Milli-Scale Gliding Arc Reactor : Investigating the Electrical and Process Parameters, *Plasma*

Chem. Plasma Process., 2016, **36**, 241–257.

26 I. B. Matveev and S. I. Serbin, Synthesis of Nitrogen Oxides in ICP / RF Plasma, *IEEE Trans. Plasma Sci.*, 2019, **47**, 47–51.

27 T. Kim, S. Song, J. Kim and R. Iwasaki, Formation of NOx from Air and N2 / O2 Mixtures Using a Nonthermal Microwave Plasma System, *Jpn. J. Appl. Phys.*, 2010, **49**, 126201.

28 S. Van Alphen, V. Vermeiren, T. Butterworth, D. C. M. Van den Bekerom, G. J. Van Rooij and A. Bogarts, Power Pulsing To Maximize Vibrational Excitation Efficiency in N2 Microwave Plasma A Combined Experimental and Computational Study, *J. Phys. Chem. C*, 2019, **124**, 1765–1779.

29 B. S. Patil, Q. Wang, V. Hessel and J. Lang, Plasma N2-fixation : 1900 – 2014, *Catal. Today*, 2015, **256**, 49–66.

30 P. Rumbach, M. Witzke, R. M. Sankaran and D. B. Go, in *Proc. ESA Annual Meeting on Electrostatics*, 2013.

31 P. Lukes, B. R. Locke and J. Brisset, in *Plasma Chemistry and Catalysis in Gases and Liquids*, 2012, pp. 243–308.

32 M. J. Traylor, M. J. Pavlovich, S. Karim, P. Hait, Y. Sakiyama, D. S. Clark and D. B. Graves, Long-term antibacterial efficacy of air plasma-activated water, *J. Phys. D. Appl. Phys.*, 2011, **44**, 472001.

33 K. Shimada, K. Takashima, Y. Kimura, K. Nihei, H. Konishi and T. Kanko, Humidification effect of air plasma effluent gas on suppressing conidium germination of a plant pathogenic fungus in the liquid phase, *Plasma Process. Polym.*, 2019, **17**, 1–15.

34 H. Jablonowski and T. von Woedtke, Research on plasma medicine-relevant plasma – liquid interaction : What happened in the past five years ?, *Clin. Plasma Med.*, 2015, **3**, 42–52.

35 K. Kucerova, Z. Machala and K. Hensel, Transient Spark Discharge Generated in Various N2/O2 Gas Mixtures: Reactive Species in the Gas and Water and Their Antibacterial Effects, *Plasma Chem. Plasma Process.*, 2020, **40**, 749–773.

36 Y. Mizukoshi, R. Katagiri, H. Horibe, S. Hatanaka, M. Asano and Y. Nishimura, Nitrogen Fixation in an Aqueous Solution by a Novel Flow Plasma System, *Chem. Lett.*, 2015, **44**, 495–496.

37 J. E. F. et al. P. J. Bruggeman, M. J. Kushner, B. R. Locke, J. G. E. Gardeniers, W. G. Graham, D. Fernandez Rivas, Plasma – liquid interactions : a review and roadmap, *Plasma Sources Sci. Technol.*, 2016, **25**, 053002.

38 M. Andrews, J. A. Raven and P. J. Lea, Do plants need nitrate ? The mechanisms by which nitrogen form affects plants, *Ann. Appl. Biol.*, 2013, **163**, 1–26.

39 N. M. Crawford, Nitrate : Nutrient and Signal for Plant Growth, *Plant Cell*, 1995, **7**, 859–868.

40 F. Horchani, R. Hajri and S. Aschi-smiti, Effect of ammonium or nitrate nutrition on photosynthesis , growth, and nitrogen assimilation in tomato plants, *J. Plant Nutr. Soil Sci.*, 2010, **173**, 610–617.

41 F. Girard, M. Peret, N. Dumont, V. Badets, S. Blanc, K. Gazeli, C. Nöel, T. Belmonte, L. Marlin, J.-P. Cambus, G. Simon, N. Sojic, B. Held, S. Arbault and F. Clément, Correlations between gaseous and liquid phase chemistries induced by cold atmospheric plasmas in a physiological buffer, *Phys. Chem. Chem. Phys.*, 2018, **20**, 9198–9210.

42 T. Ito, G. Uchida, A. Nakajima, K. Takenaka and Y. Setsuhara, Control of reactive oxygen and nitrogen species production in liquid by nonthermal plasma jet with controlled surrounding gas, *J. Appl. Phys.*, 2017, **56**, 1–6.

43 D. Xiao, C. Cheng, J. Shen, Y. Lan, H. Xie, X. Shu, Y. Meng and J. Li, Characteristics of atmospheric-pressure non- thermal N2 and N2 / O2 gas mixture plasma jet, *J. Appl. Phys.*, 2014, **115**, 033303 1–10.

44 R. H. Stark and K. H. Schoenbach, Direct current glow discharges in atmospheric air, *Appl. Phys. Lett.*, 1999, **74**, 3770–3772.

45 Z. Machala, M. Janda, K. Hensel, I. Jedlovsky, L. Lestinska, V. Foltin, V. Martisovits and M. Morvova, Emission spectroscopy of atmospheric pressure plasmas for bio-medical and environmental applications, *J. Mol. Spectrosc.*, 2007, **243**, 194–201.

46 Z. Machala, I. Jedlovský and V. Martišovitš, DC Discharges in Atmospheric Air and Their Transitions, *IEEE Trans. Plasma Sci.*, 2008, **36**, 918–919.

47 Y. P. Raizer, *Gas Discharge Physics*, 1991.

48 M. Gianella, S. Reuter, A. L. Aguila, G. A. D. Ritchie and J. H. Van Helden, Detection of HO2 in an atmospheric pressure plasma jet using optical feedback cavity-enhanced absorption spectroscopy Detection of HO 2 in an atmospheric pressure plasma jet using optical feedback cavity-enhanced absorption spectroscopy, *New J. Phys.*, 2016, **18**, 1–9.

49 S. Park, W. Choe and C. Jo, Interplay among ozone and nitrogen oxides in air plasmas : Rapid change in plasma chemistry, *Chem. Eng. J.*, 2018, **352**, 1014–1021.

50 J. Howard and I. W. Smith, Direct rate measurements on the reactions N + OH => NO + H and O + OH => O2 + H, *Chem. Phys. Lett.*, 1980, **69**, 40–44.

51 J. T. Herron and D. S. Green, Chemical Kinetics Database and Predictive Schemes for Nonthermal Humid Air Plasma Chemistry . Part II . Neutral Species Reactions 1, *Plasma Chem. Plasma Process.*, 2001, **21**, 459–481.

52 D. L. Baulch, C. J. Cobos, R. A. Cox, P. Frank, G. Hayman, T. Just, J. A. Kerr, T. Murrells, M. J. Pilling, J. Troe, R. W. Walker and J. Warnatz, Evaluated Kinetic Data for Combustion Modeling . Supplement I Evaluated Kinetic Data for Combustion Modelling Supplement I, *J. Phys. Chem. Ref. Data*, 1994, **23**, 847–1033.

53 S. Pekárek, Non-Thermal Plasma Ozone Generation, *Acta Polytech.*, 2003, **43**, 47–51.

54 M. A. Malik, C. Jiang, R. Heller, J. Lane, D. Hughes and K. H. Schoenbach, Ozone-free nitric oxide production using an atmospheric pressure surface discharge – A way to minimize nitrogen dioxide co-production, *Chem. Eng. J.*, 2016, **283**, 631–638.

55 P. Bruggeman, D. Schram, A. Manuel, R. Rego, M. G. Kong and C. Leys, Characterization of a direct dc-excited discharge in water by optical emission, *Plasma Sources Sci. Technol.*, 2009, **18**, 025017 1–13.

56 S. Iseni, R. Michaud, P. Lefaucheux and G. B. Sretenovi, micro-discharges close to atmospheric pressure On the validity of neutral gas temperature by emission spectroscopy in micro-discharges close to atmospheric pressure, *Plasma Sources Sci. Technol.*, 2019, **28**, 065003 1–15.

57 P. J. Bruggeman, N. Sadeghi, D. C. Schram and V. Linss, Gas temperature determination from rotational lines in non-equilibrium plasmas : a review, *Plasma Sources Sci. Technol.*, 2014, **23**, 023001.

58 J. Raud, M. Laan, I. Jõgi, J. Raud, M. Laan, I. J. Rotational and A. Oh, Rotational temperatures of N2 (C , 0) and OH (A , 0) as gas temperature estimates in the middle pressure Ar / O2 discharge, *J. Phys. D. Appl. Phys.*, 2011, **2**, 1–7.

59 J. Vorác, P. Synek, L. Potocnáková, J. Hnilica and V. Kudrle, Batch processing of overlapping molecular spectra as a tool for spatio-temporal diagnostics of power modulated microwave plasma jet, *Plasma Sources Sci. Technol.*, 2017, **26**, 1–12.

60 J. Vorác, P. Synek, V. Procházka and T. Hoder, State-by-state emission spectra fitting for non-equilibrium plasmas: OH spectra of surface barrier discharge at argon/water interface, *J. Phys. D Appl.*, 2017, **50**, 294002 1–14.

61 R. Sander, Compilation of Henry ' s law constants (version 4 . 0) for water as solvent, *Atmos. Chem. Phys.*, 2015, **15**, 4399–4981.

62 P. Lukes, E. Dolezalova, I. Sisrova and M. Clupek, Aqueous phase chemistry and bactericidal effects from an air discharge plasma in contact with water evidence for the formation of peroxynitrite through a pseudo second order post doscharge reaction of H2O2 and HNO2, *Plasma Sources Sci. Technol.*, 2014, **23**, 015019 1–15.

63 A. Wilson, D. Staack, T. Farouk, A. Gutsol, A. Fridman and B. Farouk, Self-rotating dc atmospheric-pressure discharge over a water-surface electrode : regimes of operation, *Plasma Sources Sci. Technol.*, 2008, **17**, 045001 1–12.

64 A. V Pipa, S. Reuter, R. Foest and K. Weltmann, Controlling the NO production of an atmospheric pressure plasma jet, *J. Phys. D. Appl. Phys.*, 2012, **45**, 085201 1–7.

65 J. G. Anderson, J. J. Margitan, F. Kaufman and J. G. Anderson, Gas phase recombination of OH with NO and NO2 Gas, *J. Chem. Phys.*, 1974, **30**, 3310–3317.

66 N. Shirai, M. Nakazawa, S. Ibuka and S. Ishii, Atmospheric DC Glow Microplasmas Using Miniature Gas Flow and Electrolyte Cathode and Electrolyte Cathode, *Jpn. J. Appl. Phys.*, 2009, **48**, 036002 1–8.

67 A. Bogaerts and E. C. Neyts, Plasma Technology : An Emerging Technology for Energy Storage, *ACS Energy Lett.*, 2018, **3**, 1013–1027.